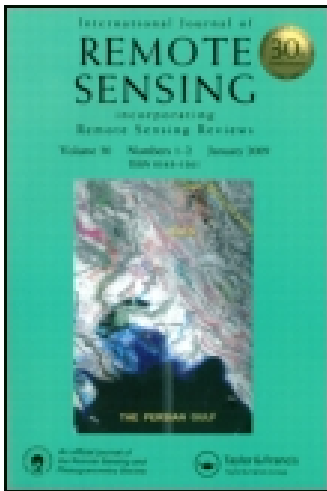


This article was downloaded by: [European Space Agency]

On: 30 July 2014, At: 04:58

Publisher: Taylor & Francis

Informa Ltd Registered in England and Wales Registered Number: 1072954 Registered office: Mortimer House, 37-41 Mortimer Street, London W1T 3JH, UK



## International Journal of Remote Sensing

Publication details, including instructions for authors and subscription information:

<http://www.tandfonline.com/loi/tres20>

### The effect of image compression on synthetic PROBA-V images

Alessandro Gimona<sup>a</sup>, Laura Poggio<sup>a</sup>, Inge Aalders<sup>a</sup> & Matt Aitkenhead<sup>a</sup>

<sup>a</sup> The James Hutton Institute, Craigiebuckler, Aberdeen AB15 8QH, UK

Published online: 27 Mar 2014.

**To cite this article:** Alessandro Gimona, Laura Poggio, Inge Aalders & Matt Aitkenhead (2014) The effect of image compression on synthetic PROBA-V images, *International Journal of Remote Sensing*, 35:7, 2639-2653, DOI: [10.1080/01431161.2014.883101](https://doi.org/10.1080/01431161.2014.883101)

**To link to this article:** <http://dx.doi.org/10.1080/01431161.2014.883101>

PLEASE SCROLL DOWN FOR ARTICLE

Taylor & Francis makes every effort to ensure the accuracy of all the information (the "Content") contained in the publications on our platform. However, Taylor & Francis, our agents, and our licensors make no representations or warranties whatsoever as to the accuracy, completeness, or suitability for any purpose of the Content. Any opinions and views expressed in this publication are the opinions and views of the authors, and are not the views of or endorsed by Taylor & Francis. The accuracy of the Content should not be relied upon and should be independently verified with primary sources of information. Taylor and Francis shall not be liable for any losses, actions, claims, proceedings, demands, costs, expenses, damages, and other liabilities whatsoever or howsoever caused arising directly or indirectly in connection with, in relation to or arising out of the use of the Content.

This article may be used for research, teaching, and private study purposes. Any substantial or systematic reproduction, redistribution, reselling, loan, sub-licensing, systematic supply, or distribution in any form to anyone is expressly forbidden. Terms & Conditions of access and use can be found at <http://www.tandfonline.com/page/terms-and-conditions>

## The effect of image compression on synthetic PROBA-V images

Alessandro Gimona\*, Laura Poggio, Inge Aalders, and Matt Aitkenhead

*The James Hutton Institute, Craigiebuckler, Aberdeen AB15 8QH, UK*

*(Received 2 November 2012; accepted 3 September 2013)*

We have carried out an in-depth investigation into the effects of image compression on synthetic Probe for On-Board Autonomy – Vegetation (PROBA-V) scenes and Landsat-derived image tiles. The two image compression implementations used were the TER implementation and a bespoke implementation of the Consultative Committee for Space Data Systems (CCSDS) Blue Book standard, which are functionally identical but operate on different image architectures. This work included (1) the development of an approach for producing synthetic scenes that were appropriate in terms of structure and content, and (2) evaluation of the image compression approach on the two kinds of image in terms of their usefulness for land-cover mapping. The synthetic image (SI) generation approach has been rigorously tested and produces images that are statistically similar to real scenes, both compressed and uncompressed. The results of our work show that the effects of image compression vary significantly between bands and with different compression ratios, and that the impact of image compression on image quality does vary with spatial scale. We also found indications of increased error rate at boundaries within the imagery. While the SI generation process and the processing chain of this imagery are not completely consistent with PROBA-V imagery, agreement was found among many of the results produced by the two approaches.

### 1. Introduction

The need to improve on-board image compression methods has been an issue for several years. Mura, Dionisio, and Oricchio (1997) highlighted, amongst other requirements, the need for effective image compression within the expanding Earth observation market of the 1990s, while Tintrup, De Natale, and Giusto (1998) compared several image compression algorithms (including Joint Photographic Experts Group (JPEG), which is an example of a discrete cosine transform (DCT), and a number of wavelet-based approaches) in an effort to identify the most effective method of reducing downlink and storage costs. Chen (1997) identified an increasing trend in the use of wavelet transforms for remote-sensing image compression. In the same year, Schwarz and Datcu (1997) investigated the potential of wavelets for a range of image-processing and archiving activities. While great improvements in both quality and standardization have taken place since then, the effects of data compression on image classification and mapping remain an issue to the present day (Addink, Van Coillie, and de Jong 2012).

Li, Yang, and Jiang (2011) and Yu and Song (2012) have demonstrated lossy and lossless image compression approaches, respectively, both based on wavelets and both suitable for satellite-based remote sensing due to low computational costs. The wavelet approach has been demonstrated to provide better data compression results than other approaches such as DCT (Nichols et al. 2009), a variant of which was used on board

---

\*Corresponding author. Email: [alessandro.gimona@hutton.ac.uk](mailto:alessandro.gimona@hutton.ac.uk)

SPOT 4 and SPOT 5 (Système Pour l'Observation de la Terre; Moury and Latry 2003). In addition to on-board lossy compression, some work has been carried out on the restoration of image data following transmission (e.g. Li and Hu 2001). This has the potential to allow the impact of high-compression ratio lossy compression to be partially or totally mitigated. However, in comparison with the development of on-board compression, this aspect has been relatively unexplored.

The on-board compression of remote-sensing imagery is a rapidly developing field, with several new and/or adapted approaches having been published in the last few years (e.g. Magli et al. 2007; Pan, Zou, and Ao 2008; Lu and Deng 2009; Jang et al. 2011) in addition to comparisons of existing approaches under different conditions (e.g. Yu, Vladimirova, and Sweeting 2009). One of the most important constraints in relation to on-board compression is available CPU power, which is limited by a combination of size, weight, and power availability conditions. Work on low-complexity image-compression algorithms is therefore a priority (Lambert-Nebout, Latry, and Moury 2001; Cagnazzo et al. 2006). Recent work (Sepehrband et al. 2011) has improved the potential of the JPEG2000 wavelet-based compression approach using an enhanced differential pulse code modulation (DPCM) transformation approach. DPCM is a method by which signals are encoded by removing the redundancy present due to positive correlations with nearby pixel values. This approach and related ones have been used a number of times for image compression (see e.g. Mozelle et al. 1997; Mielikainen and Toivanen 2003) and for compression of other spatial data sets such as digital elevation models (DEMs) (e.g. Kidner and Smith 2003).

The Consultative Committee for Space Data Systems (CCSDS) was formed in 1982 to address problems in space-based data management. Various standards (termed Blue Books) have been published by this committee in relation to the acquisition, handling, and archiving of space-related data. The CCSDS 122.0-B-1 standard describes and implements the on-board compression (lossless or lossy) of remote-sensing-acquired imagery (CCSDS 2005), based on a number of investigations and recommendations (Mozelle et al. 1998; Yeh, Moury, and Armbruster 2002). The standard is similar, but not identical to, the JPEG2000 compression approach (which was evaluated as one of the candidates for its adoption as the standard approach (Lambert-Nebout et al. 2000; Grangetto et al. 2001)). The accepted CCSDS standard has been implemented on Probe for On-Board Autonomy – vegetation (PROBA-V), and also on Formosa Satellite 5 (FORMOSAT-5), which is due to be launched in 2014 by SpaceX (Lin et al. 2010). Since its publication in 2005, further work and recommendations for the CCSDS standard on image data compression have been proposed to extend its capability in relation to quality and compression ratio, and towards hyperspectral imagery implementations (Thiebaut et al. 2007; Garcia-Vilchez and Serra-Sagrista 2009).

One of the pre-processing approaches that can be used to reduce both pixel error and image data size is 'binning', where pixels are clustered into coarser resolutions. A comparison of the relative merits of pixel binning and low compression ratios *versus* no binning and higher compression ratios to produce the same data set size concluded that overall it is preferable to use the higher compression ratios and no binning (Livens and Kleihorst 2009). This is the approach that is used on PROBA-V, but there has been little published work to show the impact of image compression on the quality and suitability of the resultant images for land cover mapping and landscape monitoring.

Zabala, Pons, and Diaz-Delgado (2006) showed that JPEG2000 lossy compression of remote-sensing imagery prior to its classification for land-cover mapping resulted in overall reduced classification accuracy as compression ratio increased. A further study (Zabala and Pons 2011) showed that this effect was minimal for areas with low

fragmentation, but that it increased with higher fragmentation. Hu et al. (2004) have shown that for areas that have low fragmentation in relation to pixel size, high compression rates (CRs) of hyperspectral imagery are also not greatly affected in relation to vegetation-relevant metrics. Zhai, Tang, and Li (2006) found that while mean pixel grey level, variance, and entropy did not change very much with compression ratio, JPEG2000 lossy compression did influence image texture. Zabala, Cea, and Pons (2012) also investigated the effect of lossy image compression on segmentation-based classification results for Quickbird imagery, and found that, while compression ratios up to a ratio of 10:1 did not increase overall classification errors by a significant amount, the shape and size of small segments could be altered.

This has potential significance for the mapping of complex landscapes with multiple land-cover types, where it is important to be able to identify not only the total area of each land-cover class but also their spatial distribution and connectivity. Li and Wu (2008) discussed the need for an approach capable of handling the complex image textures and weak local correlation of remote-sensing imagery, further highlighting the potential issues here. Possible partial solutions to this problem have been identified recently, for example by Sun et al. (2009), who developed an adaptive threshold compression approach that varies the compression ratio in accordance with image entropy. This does not, however, get past the problem that higher compression ratios may be required regardless of image entropy, due to on-board energy budgets and other technical constraints.

In this work, we investigate the impact of the image data compression algorithm to be implemented on board the PROBA-V satellite on image quality. Specifically, we investigate overall error rates and the spatial distribution of errors caused by different compression ratios. This is achieved using a combination of synthetic PROBA-V imagery generated using two different approaches, and two different implementations of the compression algorithm.

## 2. Methods

### 2.1. Generation of synthetic images

The aim of the synthetic image (SI) generation process is to produce images with local variation around a known global spatial structure. The advantage of SIs is that they have a specifiable global spatial pattern, with stochastic variations that allow for testing of the effect of variation in local spatial pattern and in length of edges. How the compression error is influenced by such factors was the main question to be answered with this approach.

We calculated the spatial structure of the SIs from the variograms and cross-variograms of four bands taken from real Landsat TM scenes. The bands used were 1, 3, 4, and 5, which correspond closely (although not perfectly) with the spectral bands used by PROBA-V. We then applied a series of steps to generate 100 realizations (i.e. 100 four-band scenes, each at 30 m resolution) that broadly respected the original global spatial structure (i.e. reproduced the variogram and cross-variograms mentioned above). The procedure employed for this was lengthy and would require more space than is available in this paper, but we have provided a summary of the procedure in the flowchart in Figure 1.

The methods used draw heavily from the geostatistical simulation literature (e.g. Goovaerts 1997, in particular Chapter 8; Cressie and Wikle 2011).

For each SI, we also reproduced the spatial pattern of the classes of the original image.

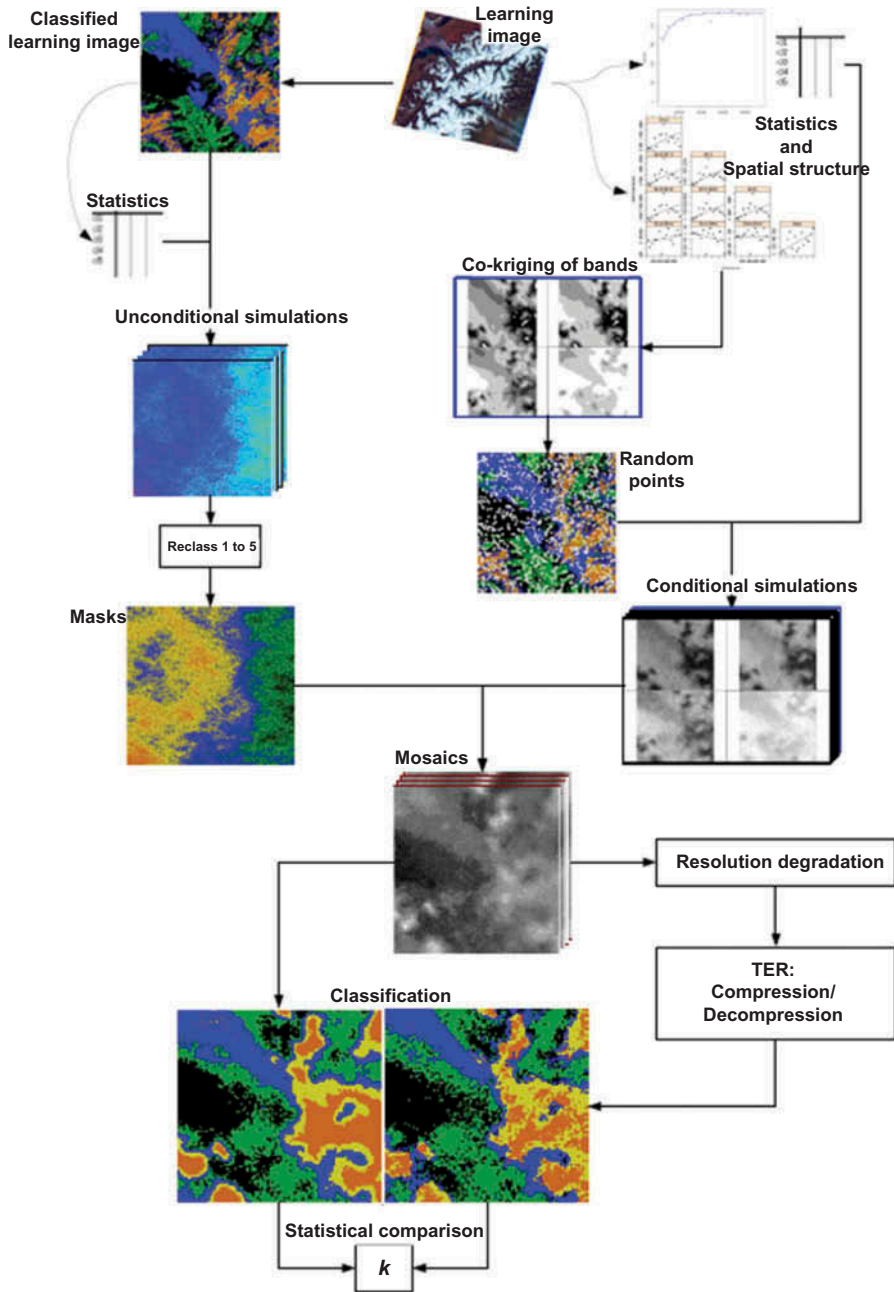


Figure 1. Flowchart of the methodology used to create SIs. TER compression here refers to the implementation of the CCSDS-122 standard. For the data handling unit (DHU) compression stage, classification was not carried out.

## 2.2. SI buffering

The rationale for creating a buffered pixel boundary around the SIs was primarily to reproduce the size of PROBA images ( $5200 \times 5200$ ) prior to compression. This was

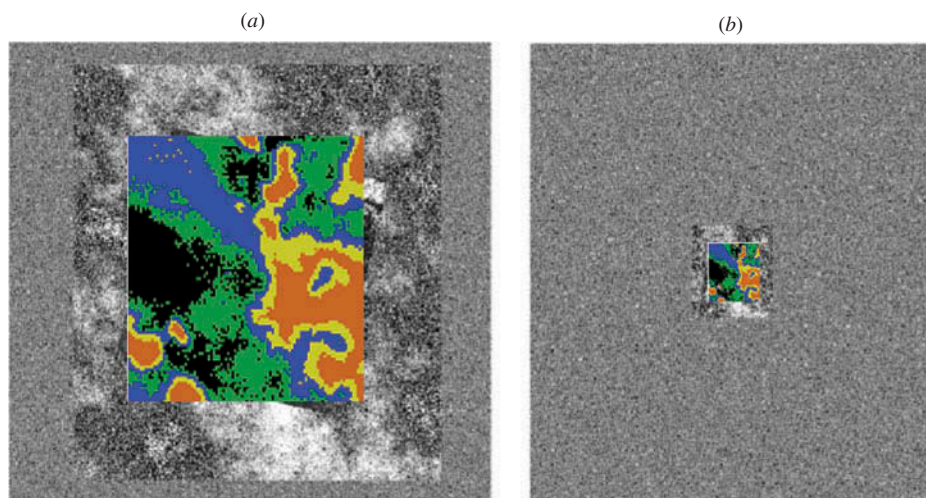


Figure 2. Example of a buffered realization. (a)  $1024 \times 1024$  pixels unconditional simulated buffer; (b)  $5200 \times 5200$  pixels uniform distributed values and  $1024 \times 1024$  pixels unconditional simulated buffer.

considered to provide a more realistic test because the compression software would work on ‘PROBA-size’ input. As it was not known what possible differences might be introduced by the compression algorithm and software through tiling of using incorrectly sized images, this stage was therefore precautionary.

Reproducing spatial patterns for large images is computationally expensive. To reduce the computation time that would have been required by creating SIs of the final size, the buffer around each SI was composed of a spatially structured part ( $1024 \times 1024$  pixels), immediately around each SI, and an unstructured part around the latter ( $5200 \times 5200$  pixels, see Figure 2). We abbreviate these images as buffered simulation images (BSIs).

### 2.3. Image degradation and CCSDS-122 standard compression

Images were degraded to reproduce more accurately the range of ground resolution of the PROBA-V pixels. We degraded the 30 m images to 300 and 1000 m prior to compression, which was not fully appropriate and reflected a lack of complete understanding of the actual PROBA-V processing chain ((A) acquisition and compression at pixel resolutions between 100 and 330 m, (B) transmission, (C) binning to resolutions between 300 and 1000 m). Our processing chain compressed pixels of lower resolution (300–1000 m) and did not include the binning step. As a result of this, further work was carried out at a later stage (see later) to ensure that accurate representation of the processing chain was incorporated into the methodology. Although the processing chain used at this point is not fully representative of the PROBA-V system, it was considered useful in providing information about trends in the impact of compression ratios on different wavelength bands and at different spatial scales.

To achieve this analysis, we therefore investigated the effects of different compression ratios on synthetic PROBA-V images at different spatial scales and on different bands, across SIs with a range of image characteristics. Each of the degraded buffered images (DBSIs) was compressed and decompressed using the TER software implementation of

the CCSDS-122 standard provided. A total of five CRs were used: 1.9, 2.4, 5.4, 7.2, and 10.8. A total of 62,500 compressed/uncompressed image pairs were analysed and compared. These were obtained from 625 permutations of CRs on different bands, with 100 SIs (realizations of the stochastic pattern) for each permutation.

#### 2.4. *Effects of compression*

The effects of image compression were assessed with regard to digital number (DN) and image classification. The root mean square error (RMSE) measure was used to compare, band by band, the DNs of the compressed bands to their corresponding uncompressed values. We also tested for differences in RMSE distributions between resolution and CRs.

For each CR, we also calculated the normalized difference vegetation index (NDVI) for each of the 100 SIs, and compared it (pixel-wise) to the original NDVI, thus obtaining a distribution of 100 values. We also mapped the median RMSE over the 100 images. For each of the resolutions above, we performed unsupervised classification of each uncompressed image and of its compressed versions. Class-wise agreement was then assessed using kappa statistics ( $\kappa$ ). The Kruskal–Wallis test was used to detect statistically significant differences among CRs.

The agreement in the ‘per pixel’ classification (i.e. the class membership) between uncompressed and compressed versions of the images was recorded. For each pixel this was defined by testing whether it belonged to the same class before and after the compression. The frequency (i.e. probability) of agreement was calculated over the 100 SIs. We also investigated which factors were able to explain the observed frequencies of agreement between images.

Morphological spatial pattern analysis (MSPA) (Soille and Vogt 2009) was used to investigate which portion of each image is more subject to misclassification due to compression. Each image was segmented into different categories prior to comparative analysis.

- (1) Core: pixels whose distance to the background is greater than the given size-parameter.
- (2) Islet: connected components that do not contain any core pixel.
- (3) Connector pixels: groups of pixels linking core-connected components.
- (4) Boundary pixels: (perforation and edge) pixels whose distance to the core pixels is lower than or equal to the given size-parameter.
- (5) Branch: pixels that do not belong to any of the previous categories. They emanate from boundaries or connectors.

#### 2.5. *Statistical analysis*

The frequency of agreement was related to MSPA, band DNs, and image texture measures, using a generalized additive modelling framework (Wood 2006). The band CR permutation and SI realization were used as random effect in separate models ( $n = 62,500$ ).

#### 2.6. *DHU compression*

Owing to concerns stated above that the SI generation process and the order in which images were processed (resampling followed by compression, rather than compression

followed by resampling), a further set of work was carried out in which image tiles of size  $352 \times 128$  pixels, with spatial resolution of 100 and 200 m were generated from Landsat scenes. A total of 12 image tiles, each with four spectral bands corresponding to the PROBA-V bands, were generated at both spatial resolutions (96 tiles in total). These tiles were compressed using the DHU compression software provided by Michael Francois and colleagues at the European Space Agency (ESA), following conversion to RAW format. The DHU package, like TER, is an implementation of the CCSDS-122 Blue Book standard, but the design difference enables more rapid compression and evaluation of single tiles than the TER package. Each tile was compressed using a bit difference of 0 (no compression), 1, 2, 3, 4, 5, 6, and 7 and then decompressed and resampled to 333 m or 666 m using bicubic interpolation. The bit differences resulted in compression ratios of 4.8, 2.4, 1.6, 1.2, 1.005, 1.0001, and 1, respectively. Comparison was made between the uncompressed and compressed tiles for individual bands, and for NDVI, but not for image classification results due to staff time allocation requirements.

### 2.7. Software used

The analyses were performed using open source software.

- (1) Geographic Resources Analysis Support System Geographic Information System (GRASS GIS) (GRASS Development Team 2012) for data management, preparation and visualization.
- (2) R software (R Core Team 2012) for the models. The following packages were used: (i) mgcv for generalized additive model (GAM) and spatially autocorrelated GAM (Wood 2006); (ii) geoR (Ribeiro and Diggle 2001) for fitting the variograms; (iii) gstat (Pebesma 2004) for kriging; and (iv) rgdal for data management (Keitt et al. 2009).

## 3. Results

### 3.1. Generation of SIs, and buffering

An example of a buffered realization is provided in Figure 2. See also the flowchart for some examples of the original and SIs. The SI is surrounded by a buffer with a similar spatial structure, while the larger ‘unconditionally simulated’ buffer has no autocorrelated spatial structure. The latter is correctly expanded in Figure 2(b).

### 3.2. Effects of compression on synthetic imagery

The CR had a statistically significant impact on DNs. Figure 3 shows the distribution of RMSE values for the different bands, resolutions, and CRs. The Kruskal–Wallis test was significant for the different resolutions and CRs, with the exception of band 5, at 1000 m.

Figure 4 presents the results for NDVI. The maps show the median RMSE values for the two resolutions. Higher values occurred along class edges. The curves show the distribution of RMSE for NDVI at different CRs and resolutions.

It should be noted that in this set of images the distributions for all CRs are very similar. Hence NDVI seems not to be affected by the CR. This could be explained if the ratio between the errors introduced in the numerator and denominator terms in the NDVI were similar across the CRs.

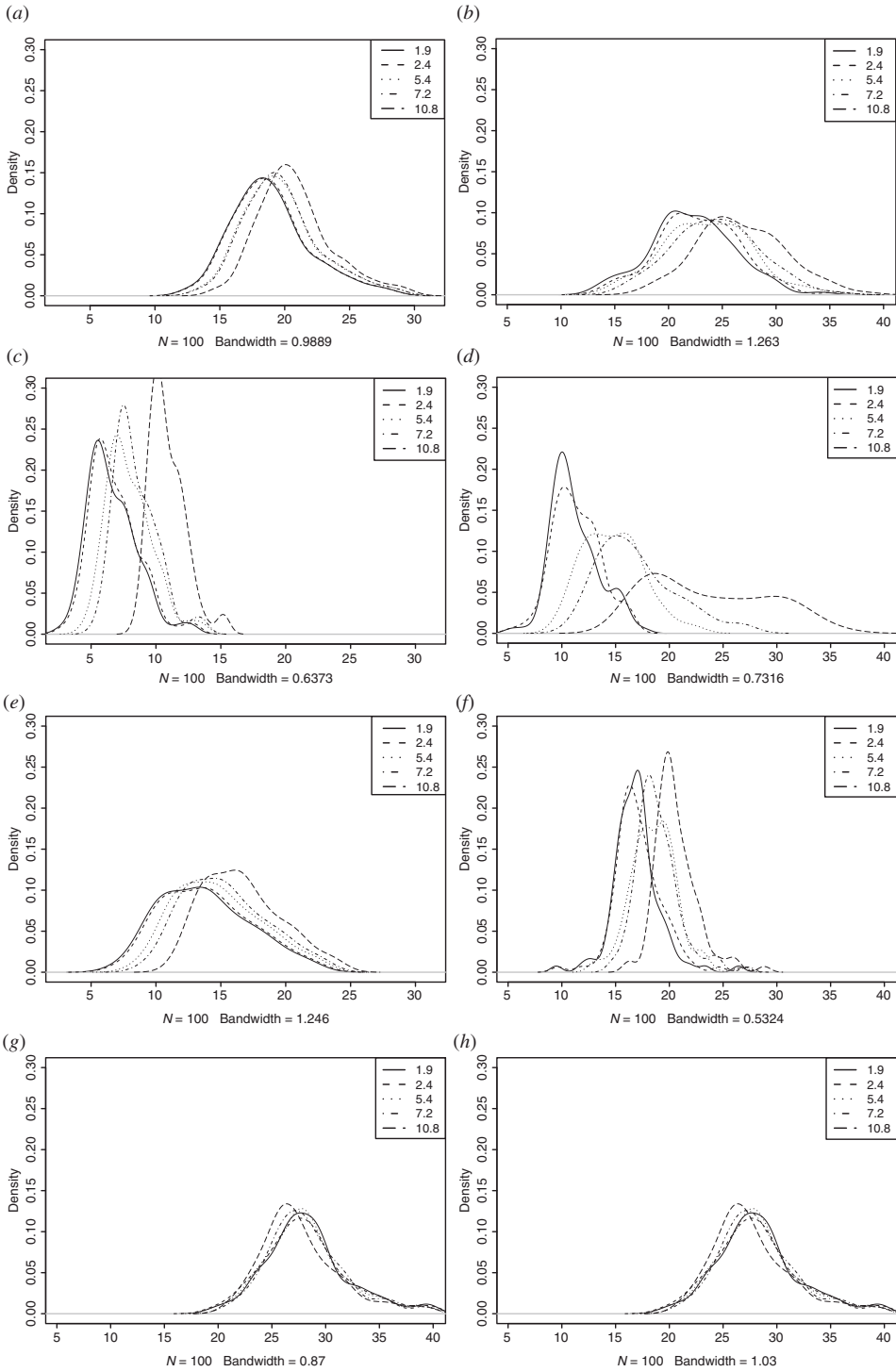


Figure 3. Distribution of RMSE values for different bands, resolutions, and CRs.

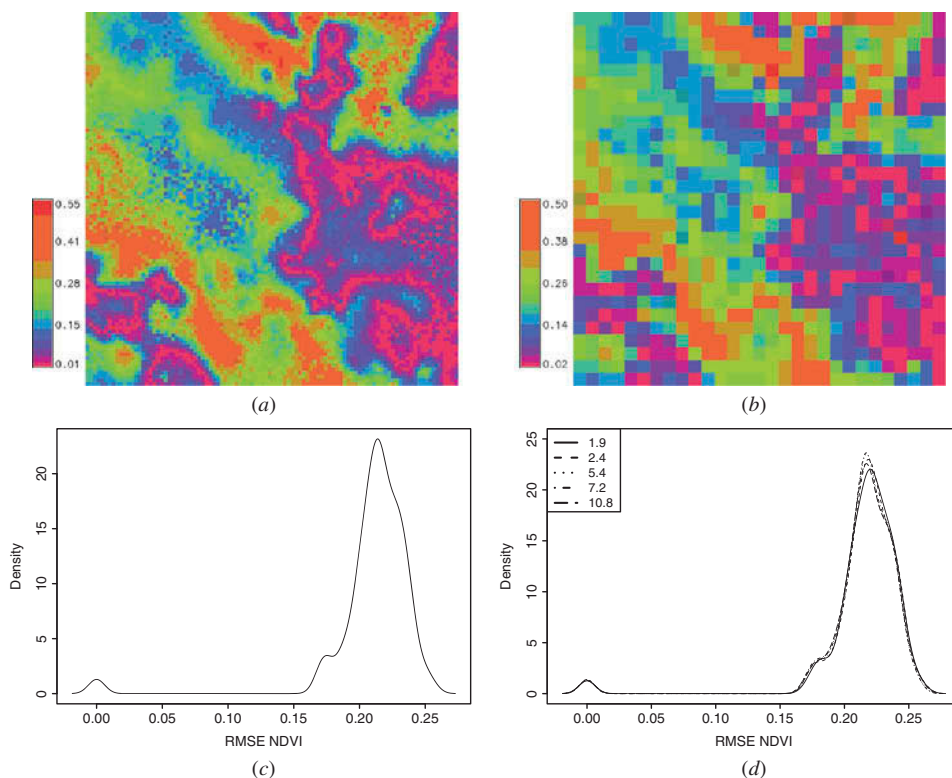


Figure 4. Maps showing median RMSE values for the two resolutions. The curves (c) and (d) show the distribution of RMSE for NDVI at different CRs and resolutions.

There was no evidence that increasing compression ratio had a significant impact on classification. The distributions of the kappa statistics for each CR are shown in Figure 5. Although the distributions appear different, their wide variability is such that the Kruskal–Wallis test results were not significant. This is because there is an image-specific effect that transcends CR (i.e. there is more variation caused by using different images than that caused by using different compression ratios).

The map of the frequency of per-pixel agreement is shown in Figure 6. The class edges appear to have higher misclassification, which was confirmed by the GAM statistical analysis that showed that the image portion had a significant effect on misclassification with MSPA ‘edges’ (islet, connector, boundary, and branch) increasing the probability of misclassification, while belonging to a ‘core area’ decreased it. Variations caused by using different SI realizations also had a significant effect indicating, again, that specific details of an image are influential on misclassification after compression. GAM plots are shown in Figure 7.

Figure 8 shows the RMSE for each of the bands across all tiles, for 100 and 200 m resampling followed by compression, decompression, and resampling to 333 or 666 m, respectively. The pixel range in these tiles is 16-bit, leading to higher absolute RMSE values than in the results above but lower proportional RMSE values.

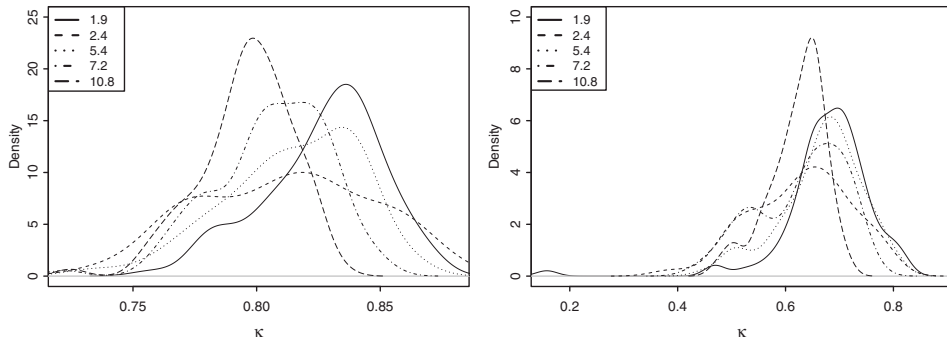


Figure 5. Distributions of the kappa statistics ( $\kappa$ ) for each CR.

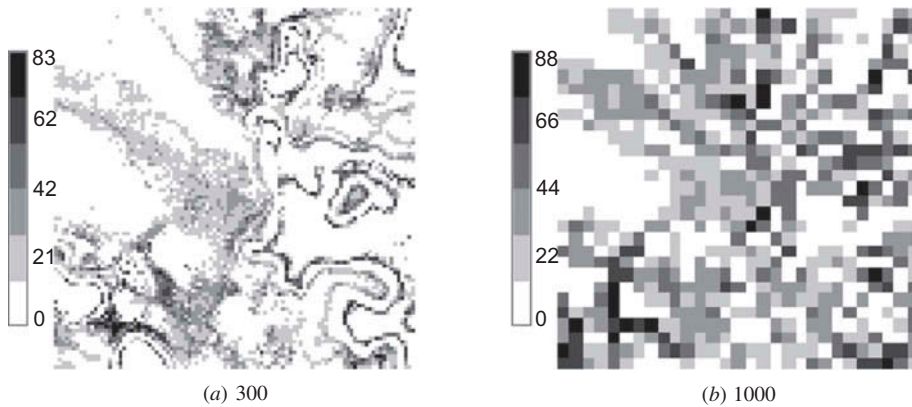


Figure 6. Map of the frequency of per-pixel disagreement.

### 3.3. DHU compression package: effects of compression

From Figure 8, it can be seen that for both image resolutions (100 and 200 m), the bands worst affected by compression are 3 and 5, while bands 1 and 4 are less affected. This is in agreement with the results given for SIs above. The DHU compression results also show a clear trend of increasing RMSE with increasing compression ratio (lower bit difference), and a clear trend of the 200 m imagery having higher RMSE values than 100 m for the same band/compression combination. Figure 9 shows the effect of different CRs on NDVI for the two spatial resolutions, and demonstrates also that at 200 m, the effects of compression on NDVI are worse than at 100 m.

A final piece of analysis on the image tiles compressed with the DHU compression tool was used to determine the correlation between pixel difference and rate of change of pixel values within the image. We found that for all bit differences of 2 or more (i.e. compression ratios of 2.4 or less), there was no statistical relationship between absolute pixel difference (between compressed and uncompressed) and the edge detection values achieved by applying a Sobel operator to the decompressed tiles ( $R^2 < 0.01$ ). However, for a bit value of 1 (CR of 4.8), there was weak correlation between pixel difference and edge detection values for 100 m resolution imagery ( $R^2$  values were between 0.03 and 0.08).

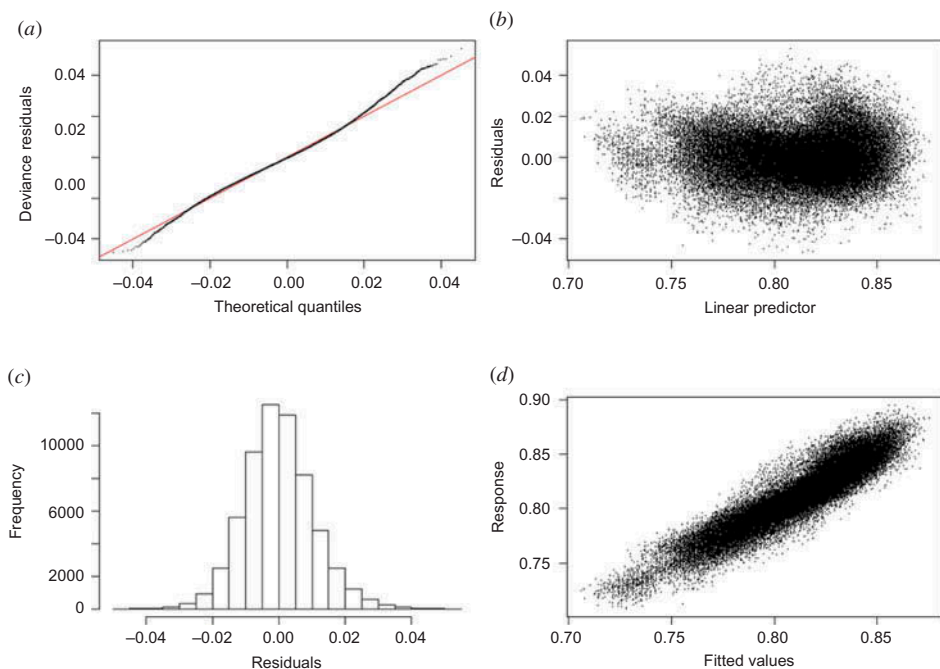


Figure 7. GAM plots: (a) residuals vs. theoretical quantiles; (b) residuals vs. linear prediction; (c) histogram of residuals; and (d) response vs. fitted values.

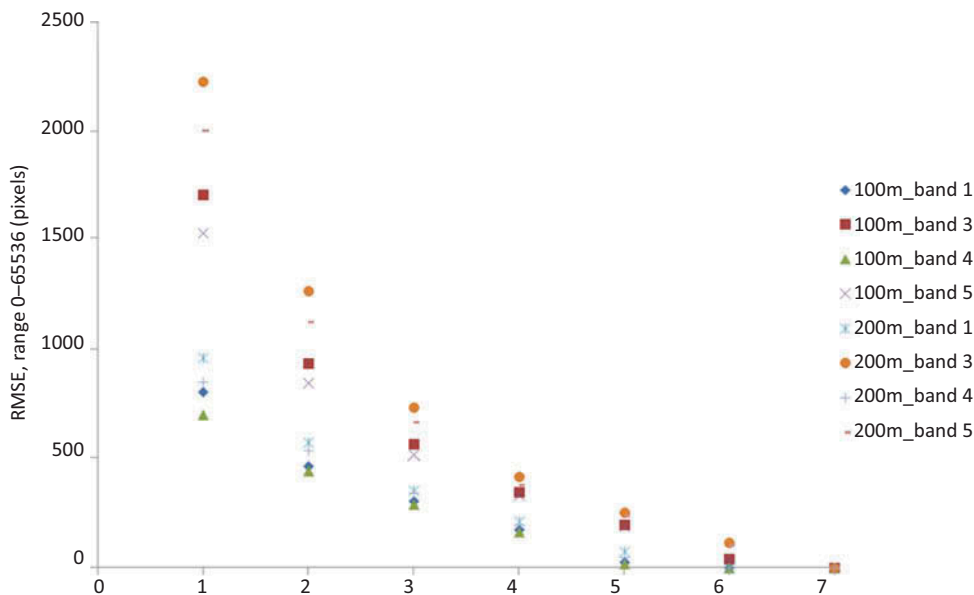


Figure 8. RMSE for bands resampled to 100 and 200 m before compression.

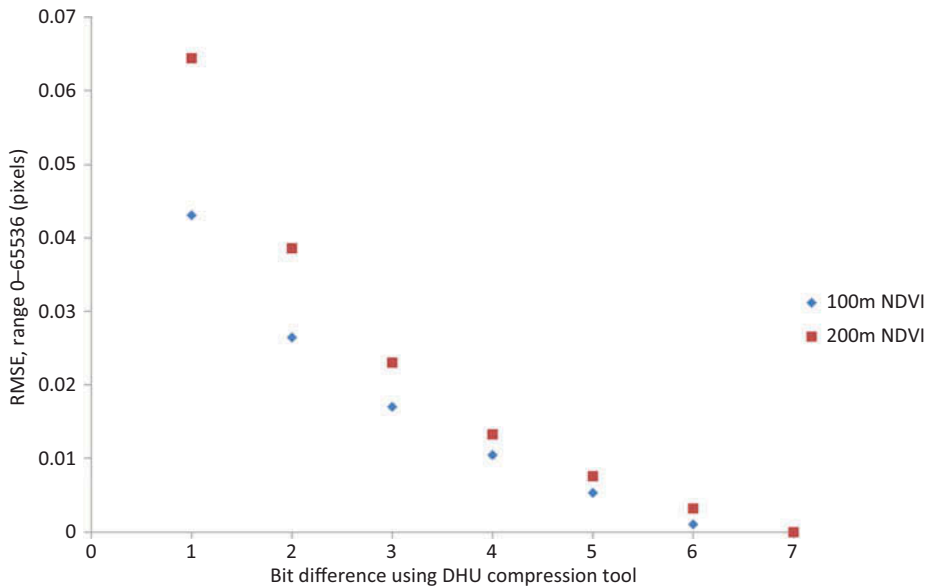


Figure 9. RMSE in NDVI for bands resampled to 100 and 200 m before compression.

This indicates that there is slightly increased error introduced at edges for high compression ratios, consistent with the results given in Figure 8 but not as strong an effect.

#### 4. Discussion

The ability of the results to represent real data sets has been tested as thoroughly as possible as part of this project, and we are confident that for the image characteristics and spatial resolutions used in our work, the measurements of image data loss are accurate for real imagery for the results obtained with the DHU compression tool. For the synthetic imagery, the effects of compression using the TER implementation of the CCSDS-122 standard are slightly greater than for compression using the DHU software package on Landsat imagery for all compression ratios, possibly due to the use of a random buffer at the edge of each image that is hard to compress. However, both methods do demonstrate that Landsat bands 3 and 5, which correspond to PROBA-V bands 2 and 4, are more strongly affected by compression than Landsat bands 1 and 4 (1 and 3 for PROBA-V). At higher or lower spatial resolutions, or for landscapes very different to those used in our evaluations (which were as broad as possible in this sense), there may be slight discrepancies between our predictions based on simulated data and the results that would be obtained on real compressed images. However, importantly, we do not think that these differences will be large enough to invite different conclusions to our work because the differences are not great and the trends in relation to compression ratio and pixel resolution are the same between the two methods.

While the SI generation process used produces imagery that may not behave under compression in exactly the same manner as real PROBA-V imagery, this approach does have advantages that would also benefit future studies. First and most importantly, the use of synthetic imagery allowed us to disentangle effects of different factors. Secondly, it was possible to produce a set of images for analysis relatively rapidly and, most significantly,

before the PROBA-V launch. One important consideration here is that comparison between synthetic and real imagery is not possible at this stage, as the sensor has not yet been launched. Further work comparing real imagery from PROBA-V to imagery from other sources should also be carried out. It would also be interesting to see whether there are any differences, however small, between simulated image data and the real thing.

From our results it seems likely that the length of edges between different land-cover classes is more influential than the CR. Therefore in some cases one could expect that more compressed but relatively more homogeneous images have less introduced error than less compressed ones if the latter have more diverse land cover and more convoluted edges.

The PROBA-V platform will definitely be able to supply imagery with a higher spatial and temporal resolution than SPOT-VEGETATION. Under many circumstances, this imagery will also be of equivalent usefulness to that from earlier platforms. However, in complex, heterogeneous landscapes where there are a large number of boundaries between different land-cover classes, there will be some increased loss of useful data at high image compression ratios. Caution should therefore be taken in inferring land-use change in these circumstances.

One of the more obvious advantages of the PROBA-V platform over existing remote-sensing platforms is the swath size; another is the frequency with which areas will be revisited. These two factors, combined with image resolution improvement over SPOT-VEGETATION, will mean potentially much more information and enhanced monitoring capabilities. These benefits must be weighed against potential losses of useful image content due to the image compression, but it is felt that on balance the benefits of using this approach are greater than the losses.

## Funding

The authors would like to thank the Belgian Science Policy Office (BELSPO) for funding this work.

## References

- Addink, E. A., F. M. B. Van Coillie, and S. M. de Jong. 2012. "Introduction to the GEOBIA 2010 Special Issue: From Pixels to Geographic Objects in Remote Sensing Image Analysis." *International Journal of Applied Earth Observation and Geoinformation* 15: 1–6.
- CCSDS. 2005. "Image Data Compression: Recommended Standard CCSDS 122.0-B-1 Blue Book." *The Consultative Committee for Space Data Systems*. CCSDS.
- Cagnazzo, M., L. Cicala, G. Poggi, and L. Verdoliva. 2006. "Low-Complexity Compression of Multispectral Images Based on Classified Transform Coding." *Signal Processing-Image Communication* 21 (10): 850–861.
- Chen, C. H. 1997. "Trends on Information Processing for Remote Sensing." In *International Geoscience and Remote Sensing Symposium (IGARSS 97) on Remote Sensing – A Scientific Vision for Sustainable Development*. Singapore: IEEE International.
- Core Team, R. 2012. *R: A Language and Environment for Statistical Computing*. Vienna: R Foundation for Statistical Computing. <http://www.R-project.org/>. ISBN 3-900051-07-0
- Cressie, N., and C. K. Wikle. 2011. *Statistics for Spatio-Temporal Data*. New York: Wiley.
- GRASS Development Team. 2012. "Geographic Resources Analysis Support System (GRASS GIS) Software." Open Source Geospatial Foundation. Accessed June 2013. <http://grass.osgeo.org>
- Garcia-Vilchez, F., and J. Serra-Sagrasta. 2009. "Extending the CCSDS Recommendation for Image Data Compression for Remote Sensing Scenarios." *IEEE Transactions on Geoscience and Remote Sensing* 47 (10): 3431–3445.
- Goovaerts, P. 1997. *Geostatistics for Natural Resources Evaluation*. New York: Oxford University Press.
- Grangetto, M., A. Caligaris, E. Magli, and G. Olmo. 2001. "JPEG2000 Evaluation for the Transmission of Remote Sensing Images on the CCSDS Packet Telemetry Channel." In *4th*

- Conference on Mathematics of Image and Data Coding, Compression, and Encryption*, edited by M. S. Schmalz. San Diego, CA: SPIE.
- Hu, B. X., S. E. Qian, D. Haboudane, J. R. Miller, A. B. Hollinger, N. Tremblay, and E. Pattey. 2004. "Retrieval of Crop Chlorophyll Content and Leaf Area Index from Decompressed Hyperspectral Data: The Effects of Data Compression." *Remote Sensing of Environment* 92 (2): 139–152.
- Jang, W. Y., M. M. Hayat, S. E. Godoy, S. C. Bender, P. Zarkesh-Ha, and S. Krishna. 2011. "Data Compressive Paradigm for Multispectral Sensing Using Tunable DWELL Mid-Infrared Detectors." *Optics Express* 19 (20): 19454–19472.
- Keitt, T. H., R. Bivand, E. Pebesma, and B. Rowlingson. 2009. "Rgdal: Bindings for the Geospatial Data Abstraction Library." Accessed June 2013. <http://CRAN.R-project.org/package=rgdal>. R package version 0.6-21
- Kidner, D. B., and D. H. Smith. 2003. "Advances in the Data Compression of Digital Elevation Models." *Computers & Geosciences* 29 (8): 985–1002.
- Lambert-Nebout, C., C. Latry, and G. Moury. 2001. "On-Board Image Compression for Space Missions." *Annals of Telecommunications* 56 (11–12): 632–645.
- Lambert-Nebout, C., C. Latry, G. Moury, C. Parisot, M. Antonini, and M. Barlaud. 2000. "On-Board Optical Image Compression for Future High Resolution Remote Sensing Systems." In *Applications of Digital Image Processing XXIII, Proceedings of the Society of Photo-optical Instrumentation Engineers (SPIE)*, Vol. 4115, 332–346. doi:10.1117/12.411557.
- Li, B., R. Yang, and H. Jiang. 2011. "Remote-Sensing Image Compression Using Two-Dimensional Oriented Wavelet Transform." *IEEE Transactions on Geoscience and Remote Sensing* 49 (1): 236–250.
- Li, Q. Q., and Q. W. Hu. 2001. "Technique of Quasi-Lossless Compression of Multiple Spectrum Remote Sensing Images Based on Image Restoration." In *Image Compression and Encryption Technologies, Proceedings of the Society of Photo-Optical Instrumentation Engineers (SPIE)*, Vol. 4551, 203–208. doi:10.1117/12.442912.
- Li, T., and W. Wu. 2008. "Remote Sensing Image Compression Based on Orientation-Adaptive Wavelet." In *2nd International Symposium on Systems and Control in Aerospace and Astronautics*, Shenzhen: People's Republic of China.
- Lin, A., C. F. Chang, M. C. Lin, L. J. Jan, and H. A. Ren. 2010. "Implementation of CCSDS Data Compression for Remote Sensing Image." In *Satellite Data Compression, Communications, and Processing VI, Proceedings of SPIE – The International Society for Optical Engineering*, Vol. 7810. doi:10.1117/12.858237.
- Liu, Y., and A. Journel. 2009. "A Package for Geostatistical Integration of Coarse and Fine Scale Data." *Computer and Geosciences* 35: 527–547.
- Livens, S., and R. Kleihorst. 2009. "Compression of Remote Sensing Images for the PROBA-V Satellite Mission." In *Proceedings of Advanced Concepts for Intelligent Vision Systems*, Lecture Notes in Computer Science 5807, 577–586. Bordeaux: ACIVS.
- Lu, L., and S. Deng. 2009. "Study on JPEG2000 Optimized Compression Algorithm for Remote Sensing Image." In *Proceedings of NSWCTC2009: International Conference on Networks Security, Wireless Communications and Trusted Computing*, Vol. 2, 771–775. doi:10.1109/NSWCTC.2009.203.
- Magli, E., M. Barni, A. Abrardo, and A. Grangetto. 2007. "Distributed Source Coding Techniques for Lossless Compression of Hyperspectral Images." *Eurasip Journal on Advances in Signal Processing*. doi:10.1155/2007/45493.
- Mielikainen, J., and P. Toivanen. 2003. "Clustered DPCM for the Lossless Compression of Hyperspectral Images." *IEEE Transactions on Geoscience and Remote Sensing* 41 (12): 2943–2946.
- Moury, G., and C. Latry. 2003. "In-Orbit Commissioning of SPOT5 Image Compression Function." In *Earth Observing Systems VIII, Proceedings of the Society of Photo-Optical Instrumentation Engineers (SPIE)*, Vol. 5151, 540–551. San Diego, CA: SPIE.
- Mozelle, G., F. Preteux, C. I. Fetita, and F. Cabot. 1997. Lossless Compression of Multispectral SPOT Images. In *Nonlinear Image Processing VIII, Proceedings of the Society of Photo-Optical Instrumentation Engineers (SPIE)*, Vol. 3026, 248–261. doi:10.1117/12/271127.
- Mozelle, G., T. Zaharia, F. Preteux, and F. Cabot. 1998. "Lossless and Nearly-Lossless Compression of Multispectral SPOT Images." In *Conference on Nonlinear Image Processing IX*, edited by E. R. Dougherty and J. T. Astola. San Jose, CA: SPIE.
- Mura, F., C. Dionisio, and D. Oricchio. 1997. "Future Remote Sensing Systems." In *17th EARSeL Symposium on Future Trends in Remote Sensing*, Lyngby, Denmark, edited by P. Gudmandsen, 17–24. Liden: AA Balkema Publishers.

- Nichols, S., H. Kim, A. A. Humos, and H. J. Cho. 2009. "A Performance Evaluation on DCT and Wavelet-Based Compression Methods for Remote Sensing Images Based on Image Content." In *17th International Conference on Geoinformatics, George Mason University, Fairfax, VA*, edited by L. Di and A. Chen, 454–458. New York: IEEE.
- Pan, W., Y. Zou, and L. Ao. 2008. A Compression Algorithm of Hyperspectral Remote Sensing Image Based on 3-D Wavelet Transform and Fractal. In *3rd International Conference on Intelligent System and Knowledge Engineering, Xiamen, People's Republic of China 2008*, edited by S. Li, T. Li, and D. Ruan, 1237–1241. New York: IEEE.
- Pebesma, E. J. 2004. "Multivariable Geostatistics in S: The Gstat Package." *Computers & Geosciences* 30: 683–691.
- Ribeiro, P. J., and P. J. Diggle. 2001. "GeoR: A Package for Geostatistical Analysis." *R-NEWS* 1 (2): 14–18. <http://CRAN.R-project.org/doc/Rnews/>
- Schwarz, G., and M. Datcu. 1997. "Wavelets – A Universal Tool for the Processing of Remote Sensing Image Data?" In *Conference on Image Processing, Signal Processing, and Synthetic Aperture Radar for Remote Sensing, London, England, 1997*, edited by J. Desachy and S. Tajbakhsh, 427–434. Bellingham, WA: SPIE.
- Sepehrband, F., P. Ghamisi, M. Mortazavi, and J. Choupan. 2011. "Simple and Efficient Remote Sensing Image Transformation for Lossless Compression." In *International Conference on Graphic and Image Processing (ICGIP), Cairo, 2011*, edited by Y. Xie and Y. Zheng. Bellingham, WA: SPIE.
- Soille, P., and P. Vogt. 2009. "Morphological Segmentation of Binary Patterns." *Pattern Recognition Letters* 30: 456–459.
- Sun, R., D. Chen, X. Li, and X. Wang. 2009. "A Remote Sensing Image Compression Algorithm Based on Adaptive Threshold." In *3rd International Symposium on Intelligent Information Technology Application, Nanchang, People's Republic of China, 2009*, edited by Q. Luo and M. Zhu, 376–378. Los Alamitos, CA: IEEE.
- Thiebaut, C., E. Christophe, D. Lebedeff, and C. Latry. 2007. "CNES Studies of on-Board Compression for Multispectral and Hyperspectral Images." In *Conference on Satellite Data Compression, Communications, and Archiving III*, Vol. 6683, edited by R. W. Heymann, B. Huang, and I. Gladkova, San Diego, CA, Article 668305. Bellingham, WA: SPIE.
- Tintrup, F., F. De Natale, and D. Giusto. 1998. "Compression Algorithms for Classification of Remotely Sensed Images." In *IEEE International Conference on Acoustics, Speech and Signal Processing (ICASSP 98)*, Seattle, WA, 2565–2568. New York: IEEE.
- Wood, S. 2006. *Generalized Additive Models: An Introduction with R*, Vol. 1, 392 p. London: Chapman and Hall/CRC Press.
- Yeh, P. S., G. Moury, and P. Armbruster. 2002. "The CCSDS Data Compression Recommendations: Development and Status." In *Conference on Applications of Digital Image Processing XXV*, Vol. 4790, edited by A. G. Tescher, Seattle, WA, 302–313. Bellingham, WA: SPIE.
- Yu, Y., and X. Song. 2012. "A Remote Sensing Image Compression Method Suited to Space-Borne Application." *International Conference on Computer Science and Network Technology (ICCSNT), Harbin Normal Univ, Harbin, People's Republic of China*, Vol. 1–4, 1132–1135. New York: IEEE.
- Yu, G., T. Vladimirova, and M. N. Sweeting. 2009. "Image Compression Systems on Board Satellites." *Acta Astronautica* 64 (9–10): 988–1005.
- Zabala, A., C. Cea, and X. Pons. 2012. "Segmentation and Thematic Classification of Color Orthophotos Over Non-Compressed and JPEG 2000 Compressed Images." *International Journal of Applied Earth Observatin and Geoinformation* 15: 92–104.
- Zabala, A., and X. Pons. 2011. "Effects of Lossy Compression on Remote Sensing Image Classification of Forest Areas." *International Journal of Applied Earth Observation and Geoinformation* 13 (1): 43–51.
- Zabala, A., X. Pons, and R. Diaz-Delgado. 2006. "Effects of JPEG and JPEG2000 Lossy Compression on Remote Sensing Image Classification for Mapping Crops and Forest Areas." *IEEE International Geoscience and Remote Sensing Symposium (IGARSS)*, Denver, CO, 790–793. New York: IEEE.
- Zhai, L., X. Tang, and L. Li. 2006. "Effects of JPEG2000 Compression on Remote Sensing Image Quality." *IEEE International Geoscience and Remote Sensing Symposium (IGARSS)*, Denver, CO, 3297–3300. New York: IEEE.